JOURNAL OF MATERIALS SCIENCE 32 (1997) 727–736

Elastic–plastic behaviour in materials loaded with a spherical indenter

A. C. FISCHER-CRIPPS*
Materials Science and Engineering Laboratory, National Institute of Standards & Technology, Gaithersburg, MD 20899, USA

Certain ceramic materials display an indentation response similar to that observed for ductile metals when loaded with a spherical indenter. This unusual behaviour, for what are nominally brittle materials, influences the mode of contact damage in applications such as machining, wear, impact damage and hardness testing. The shape of the plastic zone beneath the indenter is typically fully contained within the circle of contact on the specimen surface and thus conventional hardness theories, such as the popular expanding cavity model, provide an inadequate account of indentation response of the material. The present work demonstrates, by experiment, finite element modelling and theoretical considerations, that the indentation response is determined by the interaction between the evolving plastic zone and the mechanical properties of the specimen material, in particular, the ratio of the elastic modulus to the yield stress.

1. Introduction

Indentation tests involving hard, spherical indenters have been the basis of hardness testing since the time of Hertz in 1881 [1, 2]. Conventional indentation hardness tests involve the measurement of the size of a residual plastic impression in the specimen as a function of the indenter load. Theoretical approaches to hardness can be generally categorised according to the characteristics of indenter and the assumed response of the specimen material. For sharp indenters, the specimen is usually approximated by a rigid-plastic material in which plasticity is assumed to be governed by material flow velocity considerations. For blunt indenters, the specimen responds in an elastic–plastic manner and plastic flow is usually described in terms of the elastic constraint offered by the surrounding material. In this context, a Vickers diamond pyramid indenter would be considered blunt.

The hardness of brittle materials is conveniently measured using a diamond pyramid indenter since a residual impression is readily obtained at relatively low values of indenter load. The use of spherical indenters in hardness measurements is usually restricted to tests involving ductile materials. However, there is a class of nominally brittle materials which has been demonstrated to exhibit yield in indentation tests with spherical indenters at modest loads. For ceramic materials with a relatively large grain size and weak grain boundaries, the characteristic Hertzian cone crack normally associated with loading of a brittle material with a spherical indenter is suppressed in favour of a region of sub-surface accumulated damage [3]. One such material is the mica-containing glass–ceramic available under the trade name "Macor"†. The indentation response, as quantified by an indentation stress-strain curve, is similar to that obtained for ductile materials [4, 5]. However, the shape of the plastic zone is considerably different to that observed in metals. Rather than the commonly observed plastic zone of approximate hemispherical shape which meets the specimen surface outside the edge of the contact circle, one finds a plastic zone which, at the specimen surface, is contained within the edge of the contact circle [4, 5]. The presence of sub-surface plastic deformation and the unusual shape of the plastic zone observed in these types of materials raises questions as to the validity of established hardness theories in predicting their indentation response. Finite element modelling, experimental results and theoretical considerations are used to address these issues in the present work.

2. Theoretical considerations

2.1. General response

It is generally observed in hardness testing that the mean contact pressure beneath a Brinell (sphere) or Vickers (diamond pyramid) indenter is larger than the uniaxial compressive yield stress of the specimen material. If yield occurs due to shear, then the mean contact pressure required for bulk yield in an indentation test is higher than that required for a uniaxial compressive test because of the confining pressure generated by the surrounding elastically strained

* Guest scientist on leave from Department of Materials Science and Engineering, Lehigh University, Bethlehem, Pennsylvania 18015, USA
† Corning Inc., Corning, NY.

0022–2461

material in the indentation stress field. The ratio between the indentation mean contact pressure and the uniaxial compressive yield stress is called the constraint factor and is given the symbol C. For ductile metals, a value of $C \approx 3$ is generally considered to be appropriate [6].

Valuable information about the elastic and plastic properties of a material can be obtained with the use of a spherical indenter when the indentation stress, defined as the mean contact pressure, p_m, is plotted against the indentation strain, equal to the contact area radius, a, divided by the indenter radius, R [6]. If the radius of the indenter is large in comparison to the radius of the circle of contact with the specimen, then the indenter may be considered "blunt" and an elastic–plastic response for the specimen material assumed. The indentation stress–strain response of such a material can be generally divided into three regimes [7]:

1. $p_m < \approx Y$; fully elastic response where Y is the uniaxial yield stress of the specimen material.
2. $Y \approx < p_m < CY$; plastic deformation occurs beneath the surface but the plastic zone is completely surrounded by elastically strained material. C is the constraint factor whose value depends upon the material and the indenter geometry.
3. $p_m = CY$; plastic zone continues to grow in size such that the indentation contact area increases at a rate which gives little or no increase in the mean contact pressure for further increases in indenter load.

In Region 1, during the initial application of load, the response is elastic and can be predicted from the Hertz relation [1, 8]:

$$p_m = \left(\frac{3E}{4\pi k}\right)\frac{a}{R} \tag{1}$$

In Equation 1, k is a dimensionless constant given by:

$$k = 9/16\,[(1-\nu^2) + (1-\nu'^2)\,E/E'] \tag{2}$$

where ν and ν' are Poisson's ratio, and E and E' are Young's modulus of the specimen and the indenter respectively. Equation 1 assumes linear elasticity and makes no allowance for yield within the specimen material. For a fully elastic response, the principal shear stress for indentation with a spherical indenter is a maximum at $\approx 0.47\ p_m$ at a depth of $\approx 0.5\ a$ beneath the specimen surface directly beneath the indenter [6]. Following Tabor [6], either the Tresca or von-Mises shear stress criteria, where plastic flow occurs at $\tau_{max} \approx 0.5\ Y$, may be employed to show that plastic deformation in the specimen can be expected to first occur when $p_m \approx Y$.

Theoretical treatment of events within Region 2 is difficult because of the uncertainty regarding the size and shape of the evolving elastic–plastic zone. However, for a condition of full plasticity, semi-empirical, theoretical and finite element models which describe experimentally observed phenomena have been given considerable attention in the literature [9–21]. Generally, these models variously describe the response of the material in terms of slip lines [9], radial compressions [11–14] and elastic displacements [15, 16]. For sharp wedge or conical indenters, substantial upward flow is usually observed and since elastic strains are thus negligible compared to plastic strains, the specimen can be regarded as being rigid–plastic. A cutting mechanism is involved and new surfaces are formed beneath the indenter as the volume displaced by the indenter is accommodated by the upward flow of plastically deformed material. The constraint factor C in this case arises due to material flow and velocity considerations [9]. With blunt indenters, the mode of plastic deformation at a condition of full plasticity appears to be a result of compression rather than of cutting and the displaced volume is assumed to be taken up entirely by elastic strains within the specimen material [12, 13].

2.2. Expanding cavity model

Samuels and Mulhearn [12] and Mulhearn [13] observed that the deformation beneath a blunt wedge or conical indenter appeared to involve a radial compression mode of deformation rather than the cutting mode observed for sharp indenters. Their observations were given further attention by Marsh [11] who suggested that the deformation could be modelled using a previous analysis of Hill [10] which was concerned with the expansion of a spherical cavity in an elastic–plastic solid. The most widely accepted treatment is that of Johnson [14, 7] who considered the expansion of an incompressible hemispherical core of material subjected to an internal pressure. By specifying the volume expansion of the material at the core boundary to match that of the volume of material displaced by a conical indenter for an increment of indenter penetration into the specimen material, and by choosing the radius of the core, a_c, to be equal to the radius of the circle of contact, a, and equating the hydrostatic stress within the core to the radial stress at the core boundary, Johnson was able to express the mean contact pressure p_m as a function of the combined parameter $E/Y \tan\beta$ where β is the angle of inclination of a conical indenter to the specimen surface as shown in Fig. 1. According to Johnson [14], the mean contact pressure is given by:

$$\frac{p_m}{Y} = \frac{2}{3}\left[1 + \ln\left(\frac{(E/Y)\tan\beta + 4(1-2\nu)}{6(1-\nu^2)}\right)\right] + \frac{2}{3} \tag{3}$$

Equation 3 applies to geometrically similar indentations, such as with a conical indenter, where the radius of the plastic zone increases at the same rate as that of the core. For the case of a spherical indenter, Johnson [7] suggests that $\tan\beta$ in Equation 3 can be replaced with a/R for small values of β. However, such a procedure appears to invalidate the assumed condition of geometrical similarity. It should be noted that the expanding cavity model, as exemplified by Equation 3, invokes an elastic constraint rather than the flow constraint associated with the slip-line theory [9]. The

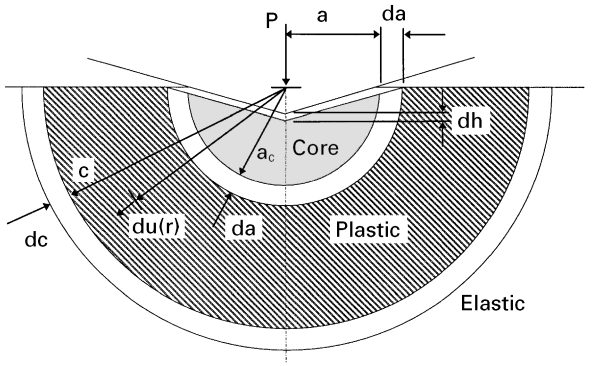

Figure 1 Expanding cavity model schematic. The contacting surface of the indenter is encased by a hydrostatic "core" of radius a_c which is in turn surrounded by a hemispherical plastic zone of radius c. An increment of penetration dh of the indenter, results in an expansion of the core da and the volume displaced by the indenter is accommodated by radial movement of particles du(r) at the core boundary. This in turn causes the plastic zone to increase in radius by an amount dc.

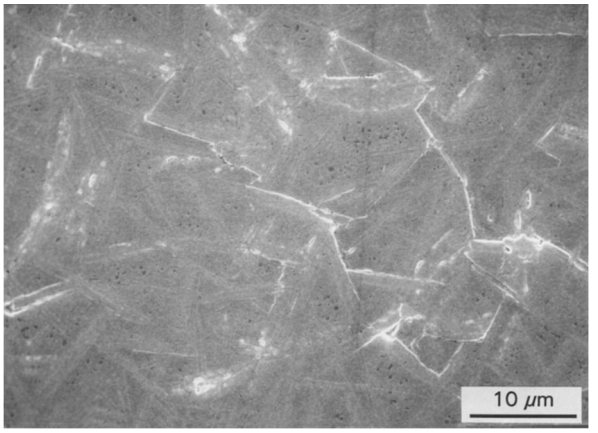

Figure 2 Electron micrograph showing shear driven failure at the mica-glass boundary. The photograph was taken at approximately position "X" in Fig. 3. Note that the orientation of the shear faults are at $\approx 90^\circ$ to each other and lie in a direction given by the Hertzian shear stress trajectories as shown in Fig. 9.

model assumes that volume displaced by the indenter is ultimately taken up by elastic strains in the bulk of the specimen and there is hence no need for upward flow. The expanding cavity model is given some attention in the present work because of its apparent enduring popularity. It will be shown later that this model should not be used beyond the scope of the restrictions imposed by its boundary conditions.

3. Experimental procedure

The elastic modulus E and the yield stress Y are two convenient parameters for characterizing the mechanical properties of an ideal elastic–plastic solid, particularly in an indentation test where the elastic and plastic properties of the specimen material are of considerable interest. In the present work, two materials have been selected for experimental study; the first, the mica-containing glass–ceramic "Macor" referred to previously, with $E/Y \approx 85$; and second, a specimen of mild steel, $E/Y \approx 550$.

The choice of a mica-containing glass–ceramic for study deserves comment. Mica-containing glass–ceramics are known for their easy machinability and yet have a respectable long-crack toughness [22]. Recent studies have shown that the nature of the damage experienced by these materials in Hertzian indentation experiments is influenced by their microstructure [4, 5]. The microstructure consists of mica platelets embedded in a glass matrix as shown in Fig. 2. If the mica platelets are larger than 2–3 μm in diameter, the indentation response is one of accumulated subsurface damage. Yielding in this material appears to be a result of shear-driven sliding of the mica-platelets within the glass matrix. Since the mica platelets are precipitated from solid solution during the heat treatment, the material is fully dense and compaction under load due to porosity is excluded. This material is of particular interest in the present work, not only because of its unusual indentation response, but because it represents a class of materials with a relatively low value for E/Y.

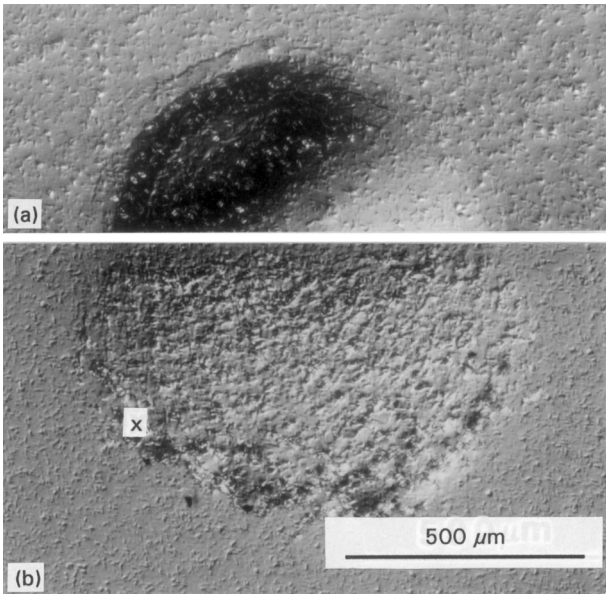

Figure 3 Bonded-interface experiment results for glass–ceramic specimen. Indenter load $P = 1000$ N, radius of indenter $R = 3.18$ mm corresponding to $a/R = 0.13$. (a) shows residual impression in the surface, (b) shows a section through the thickness of the specimen beneath the indenter. Note that the damage zone is contained within the contact circle on the specimen surface.

Indentation tests on steel with a spherical indenter have formed the basis of the well-known Brinell test since 1901 [23]. In the present work, a specimen of mild steel has been selected for testing alongside the glass–ceramic material described above. The relatively high value for E/Y for this material, together with an assumed low strain hardening characteristic, makes it suitable for such comparative testing.

Two features of the indentation process are suitable for analysis (i) the shape of the plastic zone, and (ii) the indentation stress–strain response. The shape of the plastic zone is conveniently established by the bonded-interface, or split specimen technique [24, 3]. Fig. 3 (a and b) shows the top surface and section views obtained using the procedure for a single indenter load for the glass–ceramic. Similar views are shown

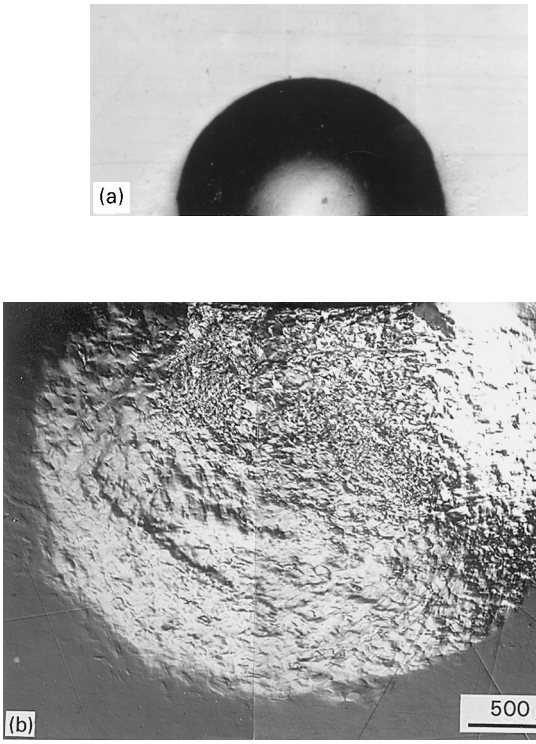

Figure 4 Bonded-interface experiment results for mild steel specimen. Indenter load $P = 1000$ N, radius of indenter $a = 3.18$ mm corresponding to $a/R = 0.18$. (a) Shows residual impression in the surface, (b) shows a section through the thickness of the specimen beneath the indenter. Note that the damage zone extends beyond the contact circle.

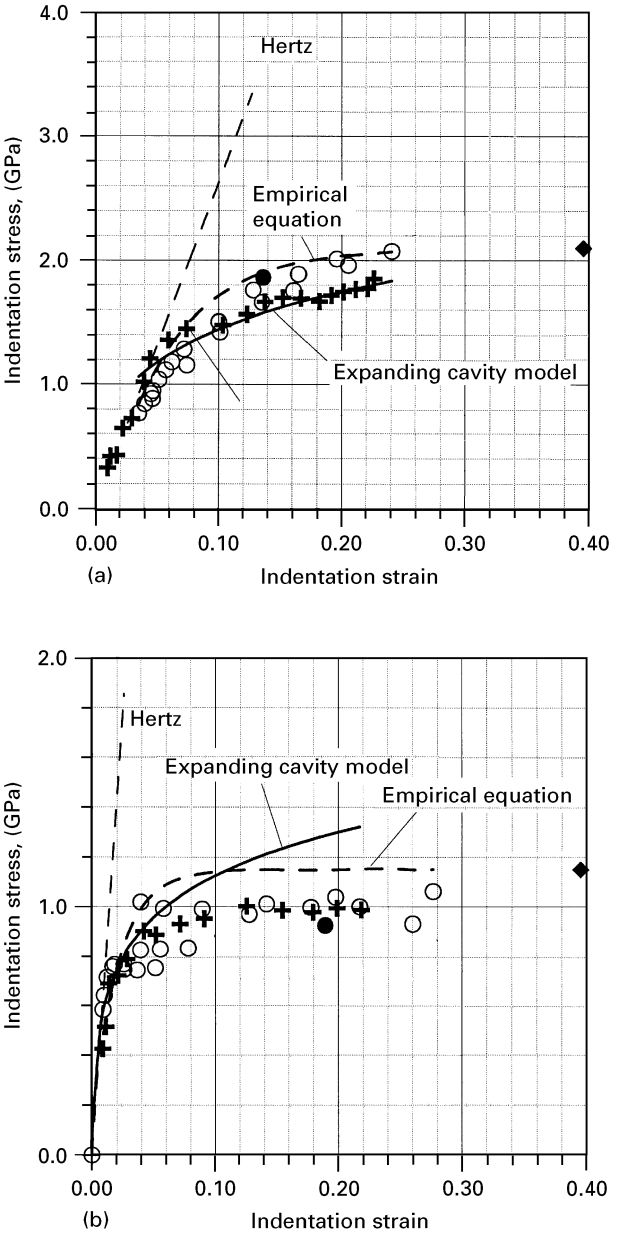

Figure 5 Indentation stress–strain response. (a) Glass–ceramic specimen with $E/Y \approx 85$ showing theoretical, finite element and experimental results. (b) Mild steel specimen with $E/Y \approx 550$. Hertzian elastic response as computed using Equation 1 is indicated for each material. (○) Indicates experimental measurements. (●) Indicates the indentation stress and strain corresponding to the bonded-interface specimens shown in Figs 3 and 4. (+) represents finite element results and (◆) at $a/R = 0.4$ represents the hardness values for each material measured with a Vickers diamond pyramid indenter. The predictions of the expanding cavity model, Equation 3 with $\tan\beta = a/R$ and the predictions of the empirical model, Equation 4 are also shown.

in Fig. 4 (a and b) for the mild steel specimen for the same load and indenter radius. The indentation stress–strain response is obtained by measuring the radius of the residual impressions left in polished, gold-coated specimens for a range of indenter loads and sizes. Although elastic recovery causes the depth, or profile, of the residual impression to be different to that when fully loaded, the radius of the impression remains virtually unchanged [14] and hence may be used to calculate the indentation stress and indentation strain for the loaded condition. Fig. 5 (a and b) shows the experimentally determined indentation stress–strain response for both the glass ceramic and the mild steel [25] materials along with finite element and theoretical results to be discussed below. The deviation from the Hertzian linear elastic response should be especially noted. Also, the slope of the initial linear portion of the curve depends upon the elastic modulus for the specimen.

Both theoretical analysis and finite element modelling of the indentation process require an estimate of the yield stress Y for the specimen material. It is of historical interest that the mean contact pressure required to initiate yield was the definition of hardness originally proposed by Hertz in 1881 [1] and may be used as an estimate of the yield stress Y. However, this method of determining Y is impractical since the onset of plasticity is a gradual process and occurs beneath the specimen surface which is normally hidden from view. Alternatively, the yield stress may be determined from the point of deviation from linearity on the indentation stress–strain curve since the mean contact pressure at this condition corresponds to $\approx Y$. This method also presents difficulties since the deviation from linearity is usually very gradual and the point of first deviation is difficult to estimate, especially for metals, where yield occurs at comparatively low values of indentation strain. However, for the glass–ceramic material considered here, there is an appreciable range of indentation strain within which there is elastic behaviour. The presence of this linear region facilitates an estimation of the point of first

TABLE I Mechanical properties of Macor and mild steel materials. Yield stress determined from experimental indentation stress–strain relationship. Hardness measured from projected area of impressions using a Vickers diamond pyramid indenter

	Young's modulus E (MPa)	Poisson's ratio ν	Yield stress Y (MPa)	E/Y	Hardness H (GPa)	Constraint factor C (H/Y)
Macor	64 000	0.26	770	85	2.1	2.7
Mild Steel	210 000	0.3	385	550	1.15	2.8

deviation from linearity. However, in practice, the results of the present work indicate that plastic flow takes place before there is a discernible deviation from linearity. Estimations of yield stress using this method are thus expected to be somewhat high. The yield stress may also be obtained from the Tabor relationship $H = CY$. For metals, $C \approx 3$ has been shown to be appropriate, but this value cannot be assumed to apply for the glass–ceramic material considered here. In consideration of all these factors, the yield stress Y for the glass–ceramic material determined from the point of deviation from linearity on the indentation stress–strain curve was considered to be adequate for the present work. A similar procedure was adopted by Swain and Hagan for soda–lime glass [26]. For the mild steel specimen, the Tabor relationship $H = 3Y$ is appropriate and the yield stress was determined from a conventional hardness measurement.

The hardness of each test specimen was measured using a Vickers diamond pyramid indenter and calculated using the projected area of contact. Tabor [6] determined experimentally that for metals which work harden, the indentation process itself corresponds to a longitudinal strain $\varepsilon \approx 8\%$ and that also, $\varepsilon \approx 0.2\, a/R$. Thus, according to this analysis, indentation with a Vickers indenter should correspond to a value of $a/R = 0.4$ for a spherical indenter. It may be expected therefore that the mean contact pressure p_m measured at $a/R \approx 0.4$ should then be equivalent to the hardness value H. However, despite the apparent convenience, it should be noted that this rule has not been demonstrated to apply, particularly to the ceramic materials considered here, thus our placing the measured hardness values at $a/R = 0.4$ in Fig. 5 is somewhat arbitrary. The measured hardness for the mild steel specimen was used to determine the yield stress Y for this material. Estimates for yield stress and hardness are given in Table I for each test material along with other mechanical properties used in the analyses.

4. Finite element analysis

Theoretical analysis of an elastic–plastic indentation with a spherical indenter is difficult because of the uncertainty regarding the shape of the evolving plastic zone. However, the problem is suitable for analysis using the finite element method where no assumption about the shape of the zone need be made beforehand. In the present work, non-linear behaviour was included by specifying an elastic perfectly plastic uniaxial stress–strain relationship as part of the property set for the elements representing the specimen where it is assumed that such a relationship is representative of that of the actual specimen material. Results for a fully linear elastic response were also calculated for verification with the Hertz elastic solution. A special feature of the present analysis is that, by the use of special gap beam elements, the expanding area of contact is accommodated automatically and no knowledge of the radius of the contact circle is required *a priori*. Elastic–plastic behaviour is modelled here by treating the specimen material as a non-linear elastic solid, hence, only the application of load may be considered. The residual field cannot be obtained directly by "unloading" but may be estimated from the difference between the elastic–plastic solution and the linear elastic solution for the fully loaded configuration [7].

The finite element analysis presented here assumes a perfectly rigid indenter in frictionless contact with the flat surface of the specimen. The finite element mesh used in the present work consisted of 1736 nodes and 1538 axis-symmetric quadrilateral plate elements. A section of the mesh near the contact is shown in Fig. 6 showing some of the gap beam elements, at points AC, used to simulate contact between the indenter and the specimen. A commercially available software package [27] was used to undertake the analysis. Elastic–plastic behaviour was accommodated by a direct iterative procedure as outlined by Zienkiewicz and Cheung [28]. In this approach, the stiffness of each element in the model is adjusted, via a secant method,[††] so that the nominated failure criterion, in this case the Tresca criterion, is satisfied within a specified tolerance level. Load is applied incrementally and it is assumed that the material behaves linearly within each increment. The dimensions of the indenter radius and the range of indenter loads in the finite element analysis matched those used in the experimental work.

Figs 7b and 8b show the shape of the evolving plastic zone as determined from the finite element analysis for the two material types. In these figures, the distance scales have been normalised to the radius of the circle of contact for the Hertzian elastic case at $P = 1000$ N for clarity. Results are shown for a range of loads from 40–1000 N applied to a 3.18 mm radius indenter. A single contour for each load step at $\tau_{max}/Y = 0.5$ has been drawn. For the purpose of investigating the dependence of the ratio E/Y of the

[††] In the secant method, the elastic modulus is given by the slope of a straight line drawn between the origin and the point on the stress–strain curve rather than the local slope of the stress–strain curve at that point.

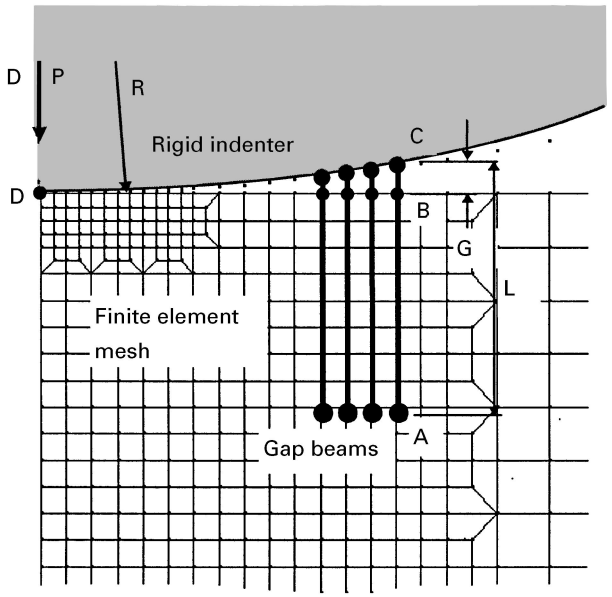

Figure 6 Finite element model showing details of mesh grading and boundary conditions. Implementation of gap beams in finite element mesh is shown. Nodes at positions B and C are constrained to move the same amount in the vertical, or z, direction so that contacting surfaces move together. Beams are maintained vertical by constraining nodes at A and C to move the same amount in the horizontal, or r, direction. Rigid indenter is modelled by constraining all nodes along the surface of the indenter at A to move the same amount in the vertical direction as the node at position D.

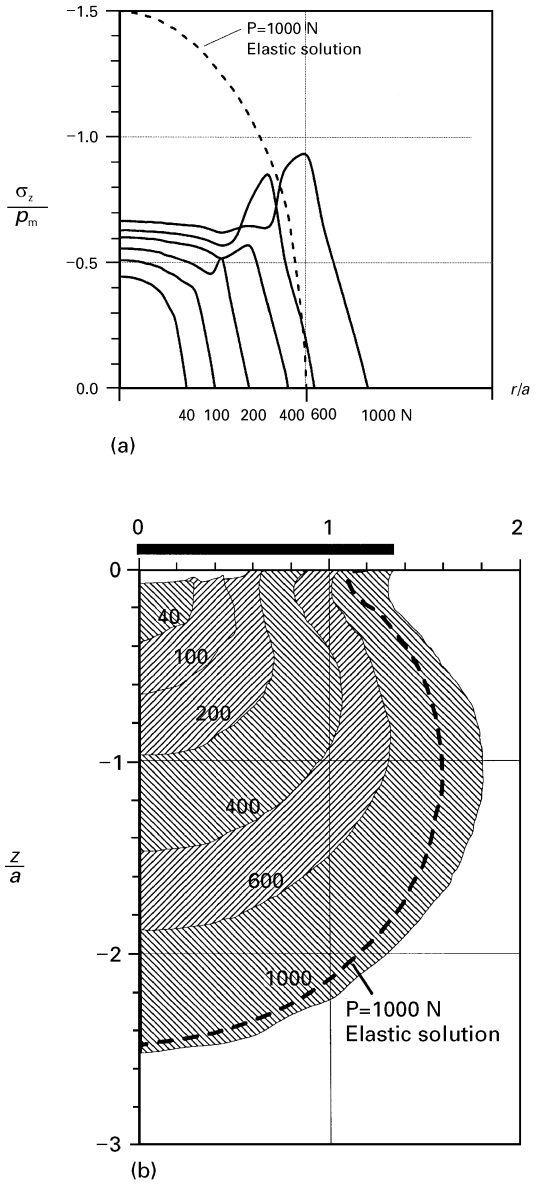

Figure 7 Finite element results showing shape of evolving plastic zone for glass-ceramic material with $E/Y \approx 85$. Results are shown for indenter loads $P = 40$, 100, 200, 400, 600 and 1000 N for $R = 3.18$ mm corresponding to indentation strains of $a/R = 0.035$, 0.05, 0.07, 0.09, 0.10, 0.13. (a) Shows the contact pressure distribution. The vertical axis is calibrated in terms of the mean contact pressure $p_m = 3.0$ GPa for the case of $P = 1000$ N. (b) Shows the development of the plastic zone in terms of contours of maximum shear stress at $\tau_{max}/Y = 0.5$. Distances are expressed in terms of the contact radius $a = 0.326$ mm for the elastic case of $P = 1000$ N. The heavy black line at the top of the lower figure indicates the radius of the circle of contact (from the F.E. solution) for $P = 1000$ N.

specimen material, an additional finite element analysis was carried out for $E/Y \approx 550$ with $E \approx 85$ GPa for comparison. The results, not shown, indicated a plastic zone similar in shape to that obtained for the case of $E = 210\,000$ MPa and $E/Y = 550$. Another solution was generated for a value of $E/Y = 200$ and the resulting shape of the plastic zone was intermediate between those shown in Figs 7b and 8b. The contact pressure distribution for each test material is shown in Figs 7a and 8a. The intersection of each of the curves in these figures with the horizontal axes in Fig. 7 (a and b) and Fig. 8 (a and b) indicates the radius of the circle of contact for each load case. The indentation stress and strain were also determined from the finite element results and plotted along with the experimental data in Fig. 5.

5. Comparisons

The predictions of various hardness theories are most markedly characterized by the proposed shape of the plastically deformed region. The expanding cavity model requires a hemispherical plastic zone coincident with the centre of contact at the specimen surface. Indeed, such a shape, for metal specimens with spherical and conical or wedge type indenters, has been widely reported in the literature [12, 13, 24] and is demonstrated approximately in the present work in Fig. 4. The finite element results shown in Fig. 7 (a and b) and Fig. 8 (a and b) demonstrate the dependence of the shape of the evolving plastic zone with respect to the mechanical properties, in particular the ratio E/Y, of the specimen material. The shapes of the plastic zones indicated in Figs 7b and 8b are consistent with those observed experimentally, as shown in Figs 3 and 4. In Fig. 7, it is shown that the shape of the plastic zone, for the case of $P = 1000$ N and $R = 3.18$ mm, predicted by the finite element analysis is similar to that of the Hertzian elastic shear stress contour corresponding to $\tau_{max}/Y = 0.5$. In Fig. 8, it is shown that the shape of the plastic zone given by the finite element analysis approaches that required by the expanding cavity model. These observations indicate that the different type of response, ranging from a contained to an uncontained plastic zone, depends on the

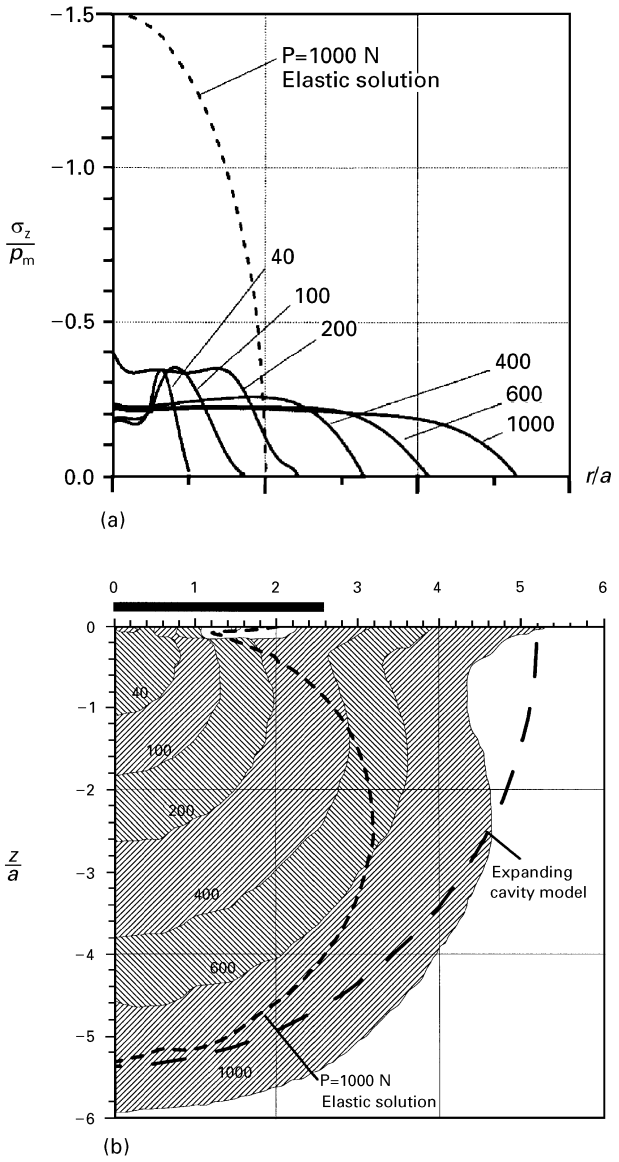

Figure 8 Finite element results showing shape of evolving plastic zone for the mild steel material with $E/Y \approx 550$. Results are shown for indenter loads $P = 40$, 100, 200, 400, 600 and 1000 N for $R = 3.18$ mm corresponding to indentation strains of $a/R = 0.04$, 0.06, 0.08, 0.11, 0.14, 0.18. (a) Shows the contact pressure distribution. The vertical axis is calibrated in terms of the mean contact pressure $p_m = 6.7$ GPa for the case of $P = 1000$ N. (b) Shows the development of the plastic zone in terms of contours of maximum shear stress at $\tau_{max}/Y = 0.5$. Distances are expressed in terms of the contact radius $a = 0.218$ mm for the elastic case of $P = 1000$ N. Also shown is the elastic–plastic boundary as predicted by the expanding cavity model with $\tan\beta = a/R$, for the case of $P = 1000$ N. The heavy black line at the top of the lower figure indicates the radius of the circle of contact (from the F.E. solution) for $P = 1000$ N.

ratio of E/Y rather than the absolute values of these terms.[§]

The indentation stress–strain response provides another comparative test for the different types of analyses. Experimental results, the predictions of the expanding cavity model, Equation 3, and the results of the finite element analysis are shown for each material in Fig. 5 (a and b). Also shown in Fig. 5 (a and b) is the linear elastic response from Equation 1. The results of the finite element analysis follow the trends indicated by the experimental results. The predictions of the expanding cavity model also follow the trends in the data but the correspondence is not particularly good.

6. Analysis

Detailed theoretical analysis of events within the specimen material is difficult because of the variable geometry of the evolving plastic zone with increasing indenter load. As load is applied to the indenter, the principal stresses σ_1 and σ_3 within the specimen material increase until eventually the flow criterion is met and thus $|\sigma_1 - \sigma_3| = Y$. An element of such material is shown at (a) in Fig. 9. Due to the constraint offered by the surrounding elastic continuum, an additional stress σ_R arises which serves to maintain the flow criterion as the load is increased. Plastic flow occurs until the magnitude of σ_R is such that, with respect to the total state of stress, the net vertical force is sufficient to balance the applied load. The total state of stress is given by the superposition of the elastic stress field and the stresses σ_R induced by the plastic deformation. Beyond the elastic–plastic boundary, the stresses σ_R follow an inverse square relationship until the stress field is substantially the same as the Hertzian elastic case, as per Saint-Venant's principle. Assuming no reverse slip [7], the stresses σ_R remain when the load is removed as the elastically strained material attempts to resume it's original configuration but is prevented from doing so by the plastically deformed material. The stresses σ_R are therefore residual stresses.

The indentation stress–strain curves determined by experiment and finite element analysis show that there is a decrease in the mean contact pressure, compared to the fully elastic case, as plastic deformation occurs beneath the indenter. For the case of a spherical indenter, a decrease in mean contact pressure, at a particular value of indenter load, corresponds to an increase in the size of the contact area and penetration depth. The observed increase in penetration depth indicates an increased energy consumption compared to the fully elastic case since the indenter load does additional work. Neglecting any frictional dissipative mechanisms, it is not immediately evident why there should be more energy transferred from the loading system into strain energy within the specimen material after plastic flow has occurred. It is quite conceivable that, *due to the elastic constraint*, plastic flow occurs and the residual stress field established without any increase in penetration depth as was thought by Shaw and DeSalvo [15, 16]. It is only the experimental evidence, in the form of a deviation from linearity on the indentation stress–strain curve, that suggests otherwise. The answer lies in the effect of plastic flow on stress distribution beneath the indenter. In Fig. 9, note that the direction of maximum shear stress for the material at position (a) is approximately 45° to the axis of symmetry and that σ_R acts in a direction

[§] Here, the term "contained" applies to the plastic zone being predominantly enclosed by elastically strained material, and "uncontained" refers to a zone which meets the surface outside the circle of contact.

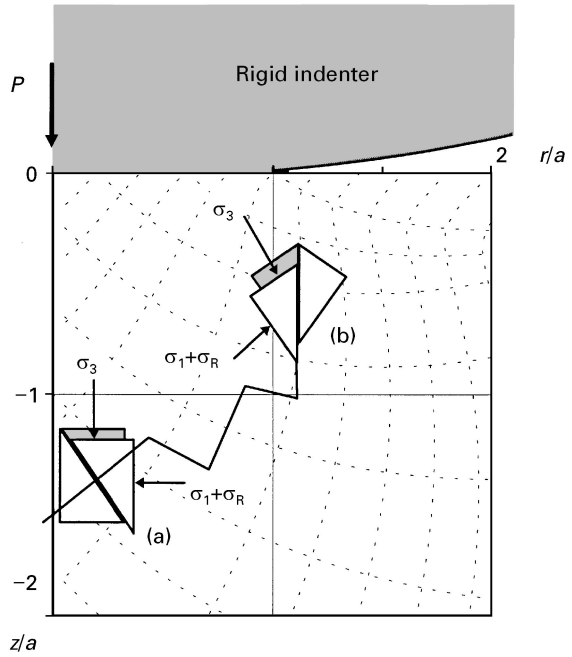

Figure 9 Schematic of plastic deformation beneath spherical indenter. Contours of maximum elastic shear stress are drawn in the background. Element of material at (a) has the direction of maximum shear oriented at approximately 45° to the axis of symmetry. Direction of maximum shear follows approximately that of the Hertzian elastic stress field for low value of E/Y. Element of material at (b) undergoes plastic deformation such that the direction of residual field supports the indenter load. Shaded areas indicate plastic strains which are ultimately taken up by elastic strains outside the plastic zone.

normal to the application of load. If it is assumed that the sliding is irreversible, i.e., plastic deformation, then the direction of σ_R at this position is such that no contribution is made by σ_R in supporting the indenter load. Rather, due to the plastic deformation at this point, the compliance of the material is increased. That is, the shaded area in Fig. 9 at (a) indicates volume of material which is taken up by *additional downwards movement* of the indenter. The displaced volume is transferred, via plastic deformation, to elastic strains in the specimen material outside the plastic zone. For the material at position (b) in Fig. 9, similar events occur but this time, the direction of maximum shear is oriented approximately parallel to the direction of applied load. Thus, at this position, the local compliance is increased due to plastic deformation, but a significant component of the residual stress σ_R tends to act in direction to support the indenter load. These observations account for the shift in the maximum of the contact pressure distribution from the centre to the points near the edge of the circle of contact, as shown in Fig. 7 (a and b), as plastic deformation proceeds. Note that the shear faults visible in the electron micrograph in Fig. 2, taken at position X in Fig. 3, are oriented at $\approx 90°$ to each other and the angle of the "fault line" is consistent with that shown in Fig. 9. In Fig. 2, little or no shear faulting is observed to occur at grain boundaries which are not aligned with the direction of maximum shear stress.

What then determines the shape of the plastic zone? For shear driven plasticity, the edge of the plastic zone coincides with the shear stress contour whose magnitude just satisfies the chosen flow criterion. The present work shows that the location of the edge of the fully developed plastic zone depends upon the ratio E/Y. The change in character from a contained to an uncontained plastic zone occurs due to the shift in the balance of elastic strain from material directly beneath the indenter outwards towards the edge of the circle of contact. As the plastic zone evolves, material away from the axis of symmetry is being called upon to take an increasing level of shear. For materials with a low value of E/Y, a large proportion of this can be accommodated by elastic strain. However, for materials with a high value of E/Y, plastic flow is comparatively more energetically favourable and thus occurs at a lower value of indenter load. The plastic zone thus takes on an elongated shape well before reaching the specimen surface and the cumulative effect is for the zone to grow ever outwards with increasing indenter load. The proximity of the specimen surface also plays a role as the material attempts to accommodate the residual field and leads to the slight "return" in the shape of the quasi-semi-circular plastic zone as shown in Fig. 7b. It is thus concluded that the semi-circular plastic zone shape associated with the expanding cavity model and observed in specimens with a high value for E/Y at high values of indentation strain arises due to the nature of the shift in elastic strain energy from material beneath, to that adjacent to the evolving plastic zone. The rate of growth of the plastic zone, with respect to increasing indenter load, affects its subsequent shape, the effect being magnified by materials with a high value of E/Y. The distribution of stress around the periphery of the plastic zone becomes more uniform as the gradients associated with the elastic stress field are redistributed as a result of plastic deformation. For both high and low ratios of E/Y, the volume displaced by the indenter is accommodated eventually by elastic strains in the specimen material. As the ratio E/Y increases, the distribution of elastic strain outside the plastic zone assumes a semi-circular shape consistent with that required by the expanding cavity model.

The expanding cavity model, which provides quantitative information about the indentation stress–strain response of the specimen material, depends upon an assumed hemispherical plastic zone and is thus restricted to materials with a relatively high value of E/Y. There has thus far been no attempt in the literature to account for the indentation stress–strain response for materials with a low value of E/Y while at the same time giving attention to the observed shapes of the plastic zone in these types of material. The indentation stress–strain responses shown in Fig. 5 (a and b) indicate a dependence on the parameters E and Y. The slope of the initial linear portion of the curve is of course directly proportional to the elastic modulus, the point of deviation from linearity corresponds approximately to an indentation stress equal to the yield stress, and the limiting value of the indentation pressure corresponds approximately to the hardness

value. This information may be used to formulate an empirical relationship between p_m and a/R. Such a relationship is given in Equation 4.

$$p_m = (C-1)Y\left(1-\exp\left[\beta\left(\frac{E}{Y}\right)^{1/2} \times\left[\frac{a}{R}-\frac{4Y\pi k}{3E}\right]\right]\right)+Y \quad (4)$$

In Equation 4, C is the constraint factor, β is a constant to be calibrated against experimental data, and k is as defined in Equation 2. Equation 4 applies to the non-linear portion of the indentation stress–strain response, i.e., $a/R > 4Y\pi k/3E$ and embodies the observed indentation stress–strain behaviour of the test specimens, as shown in Fig. 5 calculated for $\beta = 2$, but contains no information about the nature of the elastic–plastic deformation process. Such information is available from the finite element and experimental results. The usefulness of Equation 4 lies in the fact that it may be used to predict the indentation stress–strain response for a material over a wide range of indentation strains and for materials with a wide range of elastic and elastic–plastic properties.

7. Discussion

The expanding cavity model accounts for the variation of p_m with the indenter wedge angle by a consideration of the expansion of material at the core boundary with respect to the volume of material displaced by the indenter. For the case of a spherical indenter, Johnson [14, 7] suggests that $\tan\beta$ in Equation 3 can be replaced with a/R for small values of β but this violates the required condition of geometrical similarity. The geometry of the mode of deformation and the resulting relationship between p_m and E/Y $\tan\beta$ given by Equation 3 depends upon the choice of the core radius since it is this which governs the volumetric compatibility between the movement of particles on the core boundary and the material displaced by the indenter. As noted previously, in the case of a spherical indenter, yielding first occurs at some small distance beneath the surface of the specimen at some finite value of contact radius. Swain and Hagan [26] suggested that $\tan\beta$ in Equation 3 should be replaced by $(a - a^*)/R$, where a^* is the radius of the circle of contact at the onset of yield. However, this violates the volumetric compatibility implied in Equation 3. There appears to be some confusion in the literature concerning the range of applicability of the expanding cavity model. As presented by Johnson, the model is unable to predict a constant value for the constraint factor C since Equation 3 implies a monotonically increasing value of p_m with increasing a/R. At the same time, the model assumes that the plastic zone is fully developed and meets the specimen surface *outside* the circle of contact whereupon one might expect unconstrained plastic deformation. The apparent anomaly is explained by recognising that the expanding cavity model applies to relatively blunt indenters, i.e., wedges or cones with an included angle greater than $\approx 120^\circ$, or spherical indenters. The angle of the indenter is such that the flow constraint is not satisfied. The downwards movement of such an indenter causes a compression rather than the cutting action associated with a sharp indenter and no new surfaces are formed. The finite element and experimental results of the present work shows that the radial mode of deformation commonly observed [12, 13, 19, 7] in metal specimens loaded with spherical indenters occurs only at relatively high values of indentation strain. Both Johnson [7] and Chiang *et al.* [19] refer to earlier work by Samuels and Mulhearn [12] and Mulhearn [13], who observed that radial displacements within the specimen material, centred on the point of first contact, are similar for both conical and spherical indenters. It should be noted that these observations refer to work performed at relatively high values of indentation strain ($a/R = 0.51$ in reference [12]) and the later work by Mulhearn [13] deals exclusively with conical and wedge type indenters, albeit blunt, where full plasticity occurs at the point of first contact with the specimen. Under these conditions, the hemispherical plastic zone required by the expanding cavity model appears to be entirely appropriate. Marsh [11] asserts that the radial mode of compression associated with the expanding cavity model is appropriate for materials with a low value for E/Y, e.g., glasses, since it provides a relation between p_m and a/R which is consistent with experimental indentation stress–strain data. However, such a correspondence is fortuitous since, as can be seen in the present work, the shape of the plastic zone in these types of materials is inconsistent with that required by the model.

The present work demonstrates the importance of the ratio E/Y of the specimen material in predicting the indentation response of materials loaded with a spherical indenter. This is in contrast to Hardy *et al.* [17] who found that the shape of the plastic zone determined by finite element analysis was independent of E/Y, but these authors did not indicate the range of E/Y considered in their work. The mica-containing glass–ceramic material was chosen especially for study in the present work because it represents a material with a low value for E/Y relative to other materials which exhibit plastic deformation in indentation tests with spherical indenters.

Finally, it is interesting to note that the hardness number measured for the mica-containing glass–ceramic in the present work is slightly lower than the limiting value of the indentation pressure obtained from the stress–strain curve. A similar observation was made by Swain and Hagan [26] for soda-lime glass. The difference is not large however, and in general, as reported by Chiang *et al.* [19, 20], the indentation response, in the fully plastic region, may be regarded as being independent of the shape of the indenter at large values of indentation strain.

8. Conclusions

The present work shows that plastic flow beneath the spherical indenter leads to an apparent shift in elastic

strain from material beneath the indenter to that nearer to the surface, away from the centre of contact. The finite element results, supported by experimental evidence, demonstrate that there is a transition in behaviour from contained to uncontained plastic deformation with increasing value of E/Y for the specimen material. The shape of the plastic zone appears to depend on the rate of growth of the zone with respect to the indenter load. The present work brings into question the appropriateness of using theoretical models without a full consideration of the character of the indentation process with respect to the elastic–plastic properties of the specimen material, and also raises questions as to the fundamental nature of the concept of indentation hardness. In view of the difficulties associated with the evolving shape of the plastic zone in determining the indentation stress–strain relationship from first principles, an empirical relationship has been proposed which may be used to predict the indentation stress–strain response over a wide range of indentation strains and for a wide range of material types.

The present work has particular relevance to the use of ceramic materials in structural applications. Optimization of the mechanical properties for a particular application must be done at the microstructural scale where inelastic behaviour takes place. Any microstructural variation which significantly affects the macroscopic properties of the material, in particular, the ratio E/Y, influences the indentation response. For example, the geometry, or shape, of the plastic zone during impact or contact loading may lead to mechanical failure of the specimen, or alternately, may confer a degree of toughening similar to that obtained in the shot-peening of metals.

Acknowledgements

The author thanks K. Chyung of Corning Inc. for supplying the glass–ceramic materials for the experimental work for this study and also E. R. Fuller, B. R. Lawn, D. B. Marshall, N. P. Padture, and M. V. Swain for useful discussions. Funding for this work was provided by the United States Air Force Office of Scientific Research and the United States National Institute of Standards and Technology.

References

1. H. HERTZ, *J. Reine Angew. Math.* **92** (1881) 156; translated and reprinted in English in "Hertz's Miscellaneous Papers" (Macmillan, New York, 1896) Ch. 5.
2. F. AUERBACH, *Annalen de Physik* (Leipzig) **43** (1891) 61; in "Miscellaneous documents of the House of Representatives for the First Session of the Fifty-Second Congress" **43** (1891–1892) p. 207.
3. B. R. LAWN, N. P. PADTURE, H. CAI and F. GUIBERTEAU, *Science* **263** (1994) 1114.
4. H. CAI, M. A. STEVENS KALCEFF and B. R. LAWN, *J. Mater. Res.* **9** (1994) 762.
5. H. CAI, M. A. STEVENS KALCEFF, B. M. HOOKS, B. R. LAWN and K. CHYUNG, *ibid.* **9** (1994) 2654.
6. D. TABOR, "The Hardness of Metals" (Clarendon Press, Oxford, 1951).
7. K. L. JOHNSON, "Contact Mechanics" (Cambridge University Press, Cambridge, 1985).
8. M. T. HUBER, *Ann. d. Phys.* **14** (1904) 153.
9. R. HILL, E. H. LEE and S. J. TUPPER, *Proc. Roy. Soc.* **A188** (1947) 273.
10. R. HILL, "The Mathematical Theory of Plasticity" (Clarendon Press, Oxford, 1950).
11. D. M. MARSH, *Proc. Roy. Soc.* **A279** (1964) 420.
12. L. E. SAMUELS and T. O. MULHEARN, *J. Mech. Phys. Solids* **5** (1957) 125.
13. T. O. MULHEARN, *ibid.* **7** (1959) 85.
14. K. L. JOHNSON, *ibid.* **18** (1970) 115.
15. M. C. SHAW and D. J. DESALVO, *Trans. ASME* **92** (1970) 469.
16. *Idem*, *ibid.* **92** (1970) 480.
17. C. HARDY, C. N. BARONET and G. V. TORDION, *Int. J. Num. Meth. Engng.* **3** (1971) 451.
18. C. M. PERROTT, *Wear* **45** (1977) 293.
19. S. S. CHIANG, D. B. MARSHALL and A. G. EVANS, *J. App. Phys.* **53** (1982) 298.
20. *Idem*, *ibid.* **53** (1982) 312.
21. R. HILL, B. STORAKERS and A. B. ZDUNEK, *Proc. Roy. Soc.* **A423** (1989) 301.
22. D. G. GROSSMAN, *J. Amer. Ceram. Soc.* **55** (1972) 446.
23. J. A. BRINELL, in Proceedings Congrès International des Méthodes d'Essai des Matériaux de Construction, Paris, tome **2**, pp. 83–94.
24. S. R. WILLIAMS, "Hardness and Hardness Measurements" (American Society for Metals, Cleveland, Ohio, USA, 1942).
25. A. PAJARES, L. WEI, N. P. PADTURE, B. R. LAWN and C. C. BERNDT, *J. Amer. Ceram. Soc.* in press.
26. M. V. SWAIN and J. T. HAGAN, *J. Phys. D*: *Appl. Phys.* **9** (1976) 2201.
27. "Strand 6.14 Finite Element System" (G + D Computing Pty Ltd, Sydney NSW Australia, 1994).
28. O. C. ZIENKIEWICZ and Y. K. CHEUNG, "The finite element method in structural and continuum mechanics" (McGraw-Hill, London, 1967).

Received 5 July
and accepted 21 December 1995